Multistage coupling of independent laser plasma accelerators

S. Steinke[1*], J. van Tilborg[1], C. Benedetti[1], C. G. R. Geddes[1], C. B. Schroeder[1], J. Daniels[1,3], K. K. Swanson[1,2], A. J. Gonsalves[1], K. Nakamura[1], N. H. Matlis[1], B. H. Shaw[1,2], E. Esarey[1] and W. P. Leemans[1,2*]

[1]Lawrence Berkeley National Laboratory, 1 Cyclotron Road, Berkeley, California 94720, USA

[2]University of California – Berkeley, Berkeley, California 94720, USA

[3]Eindhoven University of Technology, PO Box 513, 5600MB Eindhoven, The Netherlands

*email: ssteinke@lbl.gov, wpleemans@lbl.gov

Laser-Plasma Accelerators (LPAs) are capable of providing extremely large acceleration gradients of order GeV/cm in a very compact structure[1]. However, the energy gain in a single stage LPA can be limited by laser diffraction, dephasing, electron beam loading and laser energy depletion[1]. Laser pulse guiding[2] can maintain the required laser intensity of $>10^{18}$ W cm^{-2} over multi-cm distances with the help of preformed plasma waveguides[3], dephasing can be mitigated by longitudinal tailoring of the plasma density[4], and beam loading can be controlled by proper electron beam shaping[5]. To increase the beam energy further, addressing laser energy depletion by sequencing the accelerator into stages, each powered by separate laser pulses, is also needed[6]. Here, we present results of an experiment demonstrating such staging, where two LPA stages are coupled with short separation (as is needed to preserve the average gradient) by a plasma mirror (PM). Stable electron beams from a first LPA were focused by a discharge capillary-based[7] active plasma lens[8] to a 10-micron-level beam radius into a second LPA, such that they interacted with the dark-current-free, quasi-linear wakefield excited by a separate drive laser. Staged acceleration by the wakefield of the second stage is observed via a 100 MeV energy gain for a subset of the electron beam. Changing the arrival time of the electron beam with respect to the second-stage laser pulse allowed reconstruction of the temporal field and determination of the plasma density. Our results indicate that the fundamental limitation to energy gain presented by laser depletion can be overcome using staged acceleration, which provides a path to reach electron energies required for collider applications[6,9].

A broad range of future science applications, from particle colliders beyond 1 TeV[10] to compact free-electron lasers and Thomson γ-ray sources, motivates advanced acceleration techniques such as Laser-Plasma Acceleration (LPA) to overcome the limitations of conventional accelerator technology[9]. Within the last several years tremendous progress in LPA development has been made. After the first demonstration of percent level energy spread and small divergence in mm-scale plasmas in 2004[11-13], GeV electron beams were obtained with 40 TW laser pulses[14], and subsequently electron beams with multi-GeV energies were reported with PW-class laser systems and few-cm plasmas[15-17]. Controlling the injection of electrons into plasma waves enabled precise tunability of the accelerator[18-21].

Since the accelerating gradient of a single stage LPA scales with the plasma density n_e as $E_z \propto \sqrt{n_e}$ and the single stage length is given by the laser depletion length $L_{stage} \sim L_{deplete} \propto n_e^{-3/2}$, the energy gain per stage scales as $W_{stage} \propto 1/n_e$. With the help of particle-in-cell (PIC) simulations, it was shown[22] that in order to reach an energy of 1 TeV in a single stage, a plasma density of $\sim 10^{15}$ cm^{-3} is required. This results in an acceleration length of 1 km, a low acceleration gradient,10 kJ of required laser pulse energy and a bunch not suitable for collider applications[9]. However, staging using multiple PW laser systems allows for the use of much higher plasma densities, and hence higher accelerating gradients, which results in a reduction of the total LPA-based linac length to a few hundred meters, as well as more favorable bunch charge and laser

parameters[9]. To obtain such a compact setup, coupling distances on the order of the laser depletion lengths, at the 1 m-scale, were assumed. Since the fluence restrictions of conventional laser optics requires their positioning several meters away from the focal plane of the laser, plasma mirrors[23] were proposed as final steering optics[24]. Such compact staging setup is also important to photon sources where it can be used to decelerate electrons after photon production to mitigate shielding needs[25].

Here, we demonstrate coupling of and acceleration in two separately powered LPA stages. Two synchronized laser pulses were applied to drive two acceleration stages in series (Fig. 1). The first stage generated electron beams from a gas jet target with a central energy of 120 MeV (see Methods). To maximize the coupling efficiency to the second stage, these electron beams were refocused by a first discharge capillary acting as an active plasma lens[8] to the entrance of a second discharge capillary serving as the second stage target. The acceleration fields in the second capillary were excited by the second laser pulse coupled at short distance by a PM. Dependent on the relative timing of the two laser pulses, an energy gain ~100 MeV was observed with a charge coupling efficiency of 3.5 %. Continuous scanning of the relative laser pulse timing allowed the reconstruction of the second stage wake's femtosecond-scale temporal field structure, providing an important wake diagnostic. Numerical modeling confirms the effective trapping of the electron beam in the second stage wake structure, and provides evidence for the fs duration of the first stage electron beam.

The electron beams generated in the first stage were transported to the second stage target using a pulsed active plasma lens[8]. Radially-symmetric focusing was achieved in a gas-filled 15 mm long capillary with a diameter of 500 µm using an axial discharge current of 650 A, which produced an azimuthal focusing magnetic field. The high field strengths produced (~ 0.5 T) re-focused electrons of 75−125 MeV in a distance of 25 mm through the PM tape to an energy-dependent spot size of $\sigma = 20 - 30$ µm (rms) at the second plasma stage (see inset of Fig.1). Divergence acceptance of the lens was 5mrad.

The second stage LPA target was formed by a separate discharge capillary structure (see Methods). The discharge current created a pre-formed plasma that serves as a waveguide, guiding the driving laser pulse over many Rayleigh lengths, minimizing diffraction and extending the acceleration length. These target systems are well characterized[3,14], and a model has previously been developed, permitting the determination of the wakefield amplitude by means of the spectral redshift of the transmitted laser[15,26,27]. A feedback-controlled, tape-based PM (see Methods) was used to combine the injection beam with the laser driver for the second stage.

The laser pulses reflected off the PM were guided in the parabolic plasma channel created in the discharge capillary with a transmission of 85%. Matched propagation of a transversely Gaussian laser pulse in a plasma with a transverse parabolic density profile can be obtained at low laser power and intensity if the input laser spot size, w_0(corresponding to a radius where the laser intensity is 1/e^2 compared to the on-axis value), equals the matched spot size, r_m (for a parabolic plasma profile, $n(r) = n_0 + \alpha r^2$, where n_0 is the on-axis density and α is the parameter controlling the depth the channel, the matched spot size is given by $r_m = (\alpha \pi r_e)^{-1/4}$, $r_e = 2.8 \times 10^{-13}$ cm being the classical electron radius). In our experimental conditions $r_m = 45\ \mu m$, and the laser spot size at focus was $w_0 = 18\ \mu m$, leading to mismatched propagation and, hence, to varying peak intensities and wakefield strengths along the capillary. The characteristic oscillation length of the laser spot size is given by $\lambda_{OS} = \pi z_{RM}$, where $z_{RM} = \pi r_m^2/\lambda$, and λ=0.8 µm is the central wavelength of the laser. For our parameters $\lambda_{OS} = 25$ mm. Wake excitation under these conditions was confirmed by measuring optical spectra of the transmitted laser pulse, showing an increasing redshift with increasing plasma density in the channel. Quantitative analysis of the spectra revealed a maximum relative redshift of 3% with respect to the central wavelength of the laser at a density of 2×10^{18} cm^{-3} . This corresponds to an average field amplitude of ~17 MV/mm if wake excitation occurs over the full length of the capillary[26].

To control the phasing of the electron beam in the plasma wake of the second stage LPA, the delay between the two laser pulses driving the first- and the second stages was varied with fs precision by an optical delay stage in the laser beam line of the injector stage. Electron spectra were recorded as a function of the delay between the two laser pulses. In the case of a positive delay, the first stage electrons propagated without the influence of the second laser pulse. After the second laser pulse arrived (negative delay), the electron spectra were periodically modulated in energy (Fig. 2a). The period of the modulation was (80 ± 6) fs, consistent with a plasma wavelength $\lambda_p = 24$ µm at a density of $(1.9 \pm 0.3) \times 10^{18}$ cm^{-3}.

The constant periodicity of the observed modulation as a function of delay behind the driver pulse further indicates a quasi-linear wake, consistent with expectations for the experimental parameters including laser intensity and plasma density.

To investigate the influence of the second stage wakefield on the electron beam in detail, a reference spectrum of an unperturbed beam (positive delay) was subtracted from the spectrum at each delay to emphasize the effect of the second laser pulse while maintaining absolute charge information. The resulting electron distributions are plotted in Fig. 2b in the form of a waterfall plot of electron spectra where each horizontal line corresponds to a 5-shot averaged energy spectrum. Background-subtracted 2D charge maps, also averaged over 5 shots, are shown in Fig. 2d-g for significant delays. The presence of the second-stage laser results in a reduction of total beam charge of up to a factor of 3 (see Fig. 2a). For appropriate timing of the second stage laser, however, charge was detected beyond the energy cut-off of the input electron spectrum, i.e. >200 MeV. This charge accelerated beyond the cutoff of the input spectrum, shown by the red and yellow areas in Fig. 2b,d,f, indicates acceleration in the second stage. The integrated charge in this region of 1.2 pC represents the charge trapped in the accelerating phase of the wake and respectively, a trapping efficiency of 3.5%. At delays of $\lambda_p/2$ after the times of maximum energy gain, ~1 pC of additional charge was detected around 110−150 MeV (Fig. 2e,g). This could correspond to electrons decelerated or to electrons deflected by the transverse wake fields into the spectrometer acceptance. The broad energy spread of the first stage electron beam prevents unambiguous observation of the decelerating phase of the wake under these conditions.

Numerical modelling performed with the code INF&RNO[28,29] allows detailed analysis of the interaction. Fig. 3a shows reference-subtracted electron spectra as a function of the delay between the arrival of the electron bunch and the laser pulse. The simulations show that the observed energy modulations depend on the phasing of the electron bunch within the wake. The periodicity of the modulation is determined by the plasma density and is consistent with the experimental observation. However, the amount of post accelerated charge decreases in the later accelerating phases of the wake as a result of an increasing wake curvature. The fact that the linearity of the wake appears to be preserved in the experimental results could be attributed to a deviation from the parabolic plasma channel. It was shown that e.g. a quartic plasma density profile yields a charge distribution similar to that obtained in the experiment (see extended data figure 1). Simulations performed assuming matched guiding conditions, and a more energetic injector beam with reduced energy spread, indicate that ~90% trapping can be achieved (see extended data figure 2).

As discussed above, there were two regions of increased laser intensity, and hence higher wake amplitude, in the capillary due to mismatched laser pulse guiding. The evolution of electron energy (Fig. 3b) and bunch size (Fig. 3c) are plotted as function of propagation in the capillary for two different electron populations at a delay of -252 fs: electrons that had an initial energy in the interval 75-125 MeV did not gain a significant amount of energy, and they were strongly defocused by the transverse wakefield in the early stages of the laser plasma interaction. On the other hand, electrons with a final energy above 200 MeV experienced a ~100 MeV energy gain in the vicinity of the 2nd laser focus, corresponding to a propagation distance of z = 24-29 mm in the plasma, where, due to the focusing induced by the discharge current and the laser-induced wake, they reach a spot-size of ~5 µm and interact strongly with the laser-driven plasma wake. This is shown Fig. 3c, where we plot (red solid line) the evolution of the transverse electron bunch size as a function of the propagation distance. The red dashed line in the same figure shows the evolution of the bunch spot size without the influence of the laser pulse, indicating that the contribution of the external magnetic field induced by the discharge current of the second capillary on the trapping of the electrons cannot be neglected. To elucidate this, we computed the amplitude of the transverse force, $F_\perp(z)$, acting on the electron bunch at a distance of 10 µm and 20 µm from the capillary axis in the simulation. The focusing contribution from the externally applied discharge current is given by $F_\perp(z=0)$, where no wake contribution is present. The ratio $F_\perp(z)/F_\perp(z=0)$ is plotted in Fig. 3d. For propagation distances in the capillary of z<10 mm, the average spot size of electrons with final energies of 200 – 300 MeV is larger than w_0 and hence, the external field prevails and focuses the electron beam. At positions $10\ \text{mm} < z < 22\ \text{mm}$, the laser intensity is significantly reduced due to mismatched guiding (Fig. 3b) and hence, the focusing force from the externally applied current is of the same order as the wakefield contribution, leading to continued focusing of the electron beam. Finally, for $24\ \text{mm} < z < 29\ \text{mm}$, the contribution of the wakefield dominates the interaction. In this range, a subset of the electron beam is trapped in the wakefield and gains energy. An energy gain of ~100MeV is observed in the simulations. For consistency purposes, the experiment was repeated with the

reversed, i.e. defocusing current in the second capillary. In case of a defocusing current in the second capillary, the external focusing field that supports trapping in the region ($24\text{mm} < z < 29\text{mm}$) is absent. Trapping still occurs in the region of the first laser focus ($2\text{mm} < z < 5\text{mm}$) but electrons trapped here are subsequently dephasing/ de-focuing and hence, do not experience a detectable energy gain at the end of the second capillary. The full dataset set is shown in extended data figure 3.

In summary, we have presented an experimental study of staging of two LPAs independently driven by two synchronized laser pulses. Electron beam injection and capture into the second stage wake was demonstrated by means of an ~100 MeV energy gain recurring at delays corresponding to multiples of λ_p. The observation of temporally well-defined energy modulations further directly implies a bunch length of the input electron beam shorter than $\lambda_p/4 \sim 5$ μm. This represents a major milestone in the development of laser driven plasma-based accelerators towards future colliders, as well as any other LPA application that requires electron energies beyond the single-stage limits. Simulations of modules that provide multi-GeV energy boosts to high quality electron beams by operating at lower densities (i.e., larger transverse wake size) suggest that 100% trapping can be achieved. The demonstration of such collider relevant stages including timing synchronization of separate laser drivers will be the focus of future work.
.

References

1 Esarey, E., Schroeder, C. B. & Leemans, W. P. Physics of laser-driven plasma-based electron accelerators. *Reviews of Modern Physics* **81**, 1229-1285, (2009).

2 Durfee, C. G. & Milchberg, H. M. Light pipe for high intensity laser pulses. *Physical Review Letters* **71**, 2409-2412, (1993).

3 Spence, D. J. & Hooker, S. M. Investigation of a hydrogen plasma waveguide. *Physical Review E* **63**, 015401, (2001).

4 Rittershofer, W., Schroeder, C. B., Esarey, E., Gruner, F. J. & Leemans, W. P. Tapered plasma channels to phase-lock accelerating and focusing forces in laser-plasma accelerators. *Physics of Plasmas* **17**, 063104, (2010).

5 Schroeder, C. B., Benedetti, C., Esarey, E. & Leemans, W. P. Beam loading in a laser-plasma accelerator using a near-hollow plasma channel. *Physics of Plasmas* **20**, 123115, (2013).

6 Leemans, W. P. & Esarey, E. Laser-driven plasma-wave electron accelerators. *Phys Today* **62**, 44, (2009).

7 Gonsalves, A. J., Rowlands-Rees, T. P., Broks, B. H. P., van der Mullen, J. J. A. M. & Hooker, S. M. Transverse Interferometry of a Hydrogen-Filled Capillary Discharge Waveguide. *Physical Review Letters* **98**, 025002, (2007).

8 van Tilborg, J. *et al.* Active Plasma Lensing for Relativistic Laser-Plasma-Accelerated Electron Beams. *Physical Review Letters* **115**, 184802, (2015).

9 Schroeder, C. B., Esarey, E., Geddes, C. G. R., Benedetti, C. & Leemans, W. P. Physics considerations for laser-plasma linear colliders. *Phys Rev Spec Top-Ac* **13**, 101301, (2010).

10 Ellis, J. & Wilson, I. New physics with the compact linear collider. *Nature* **409**, 431-435, (2001).

11 Geddes, C. G. R. *et al.* High-quality electron beams from a laser wakefield accelerator using plasma-channel guiding. *Nature* **431**, 538-541, (2004).

12 Mangles, S. P. D. *et al.* Relativistic electron accleration by a laser of intensity in excess of 10(20) W cm(-2). *Phys Scripta* **T107**, 121-124, (2004).

13 Faure, J. *et al.* A laser-plasma accelerator producing monoenergetic electron beams. *Nature* **431**, 541-544, (2004).

14 Leemans, W. P. *et al.* GeV electron beams from a centimetre-scale accelerator. *Nature Physics* **2**, 696-699, (2006).

15 Leemans, W. P. *et al.* Multi-GeV Electron Beams from Capillary-Discharge-Guided Subpetawatt Laser Pulses in the Self-Trapping Regime. *Physical Review Letters* **113**, 245002, (2014).

16 Wang, X. M. *et al.* Quasi-monoenergetic laser-plasma acceleration of electrons to 2 GeV. *Nature Communications* **4**, 1988, (2013).

17 Kim, H. T. *et al.* Enhancement of Electron Energy to the Multi-GeV Regime by a Dual-Stage Laser-Wakefield Accelerator Pumped by Petawatt Laser Pulses. *Physical Review Letters* **111**, 165002, (2013).

18 Gonsalves, A. J. *et al.* Tunable laser plasma accelerator based on longitudinal density tailoring. *Nature Physics* **7**, 862-866, (2011).

19 Faure, J. *et al.* Controlled injection and acceleration of electrons in plasma wakefields by colliding laser pulses. *Nature* **444**, 737-739, (2006).

20 Liu, J. S. *et al.* All-Optical Cascaded Laser Wakefield Accelerator Using Ionization-Induced Injection. *Physical Review Letters* **107**, 035001, (2011).

21 Amiranoff, F. *et al.* Observation of laser wakefield acceleration of electrons. *Physical Review Letters* **81**, 995-998, (1998).

22 Vay, J. L. *et al.* Modeling of 10 GeV-1 TeV laser-plasma accelerators using Lorentz boosted simulations. *Physics of Plasmas* **18**, 123103, (2011).

23 Thaury, C. *et al.* Plasma mirrors for ultrahigh-intensity optics. *Nature Physics* **3**, 424-429, (2007).
24 Sokollik, T. *et al.* Tape-drive Based Plasma Mirror. *AIP Conference Proceedings* **1299**, 233-237, (2010).
25 Powers, N. D. *et al.* Quasi-monoenergetic and tunable X-rays from a laser-driven Compton light source. *Nat Photonics* **8**, 29-32, (2014).
26 Shiraishi, S. *et al.* Laser red shifting based characterization of wakefield excitation in a laser-plasma accelerator. *Physics of Plasmas* **20**, 063103, (2013).
27 Andreev, N. E. *et al.* Analysis of laser wakefield dynamics in capillary tubes. *New J. Phys.* **12**, 045024, (2010).
28 Benedetti, C., Schroeder, C. B., Esarey, E., Geddes, C. G. R. & Leemans, W. P. Efficient Modeling of Laser‐Plasma Accelerators with INF&RNO. *AIP Conference Proceedings* **1299**, 250-255, (2010).
29 Benedetti, C., Schroeder, C. B., Esarey, E. & Leemans, W. P. Efficient modeling of laser-plasma accelerators using the ponderomotive-based code INF&RNO. *Proceedings of ICAP2012, Rostock-Warnemünde, Germany, 2012 (JACoW, Geneva, 2012)*, THAAI2, (2012).

Acknowledgements

The authors thank S. Shiraishi and T. Sokollik for their contributions to the initial construction of the setup and an early version of the experiment, as well as C. Toth, D. Syversrud, N. Ybarrolaza, M. Kirkpatrick, G, Mannino, T. Sipla, D. Evans, R. Duarte, D. Baum, D. Munson for their contributions. This work was supported by the U.S. Department of Energy Office of Science Office of High Energy Physics, under Contract No. DE-AC02-05CH11231, by the U.S. Department of Energy National Nuclear Security Administration, Defense Nuclear Nonproliferation R&D (NA22) and by the National Science Foundation (NSF) under contracts 0917687 and 0935197. This research used computational resources (Edison, Hopper) of the National Energy Research Scientific Computing canter (NERSC), which is supported by the Office of Science of the U.S. Department of Energy under Contract No. DE-AC02-05CH11231.

Author Contribution

All authors contributed extensively to the work presented in this paper.

Author Information

Reprints and permissions information is available at www.nature.com/reprints. The authors declare no competing financial interests. Readers are welcome to comment on the online version of the paper. Correspondence and requests for materials should be addressed to S.S. or W.P.L (ssteinke@lbl.gov, wpleemans@lbl.gov).

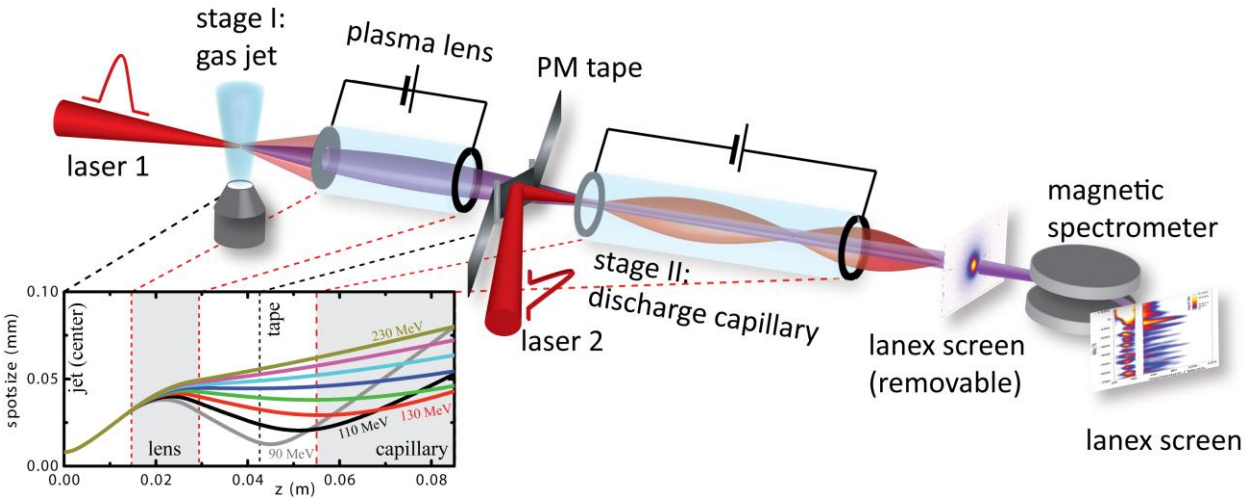

Figure 1 Concept of the experimental setup. The inset shows the evolution of the electron beam waist simulated for different energies including scattering in the tape along the beam path (z) according to Ref. 35. Energies in the interval 75-125 MeV are focused at the entrance of the stage 2 capillary to spotsizes on the order of the laser w_0 = 18µm**.**

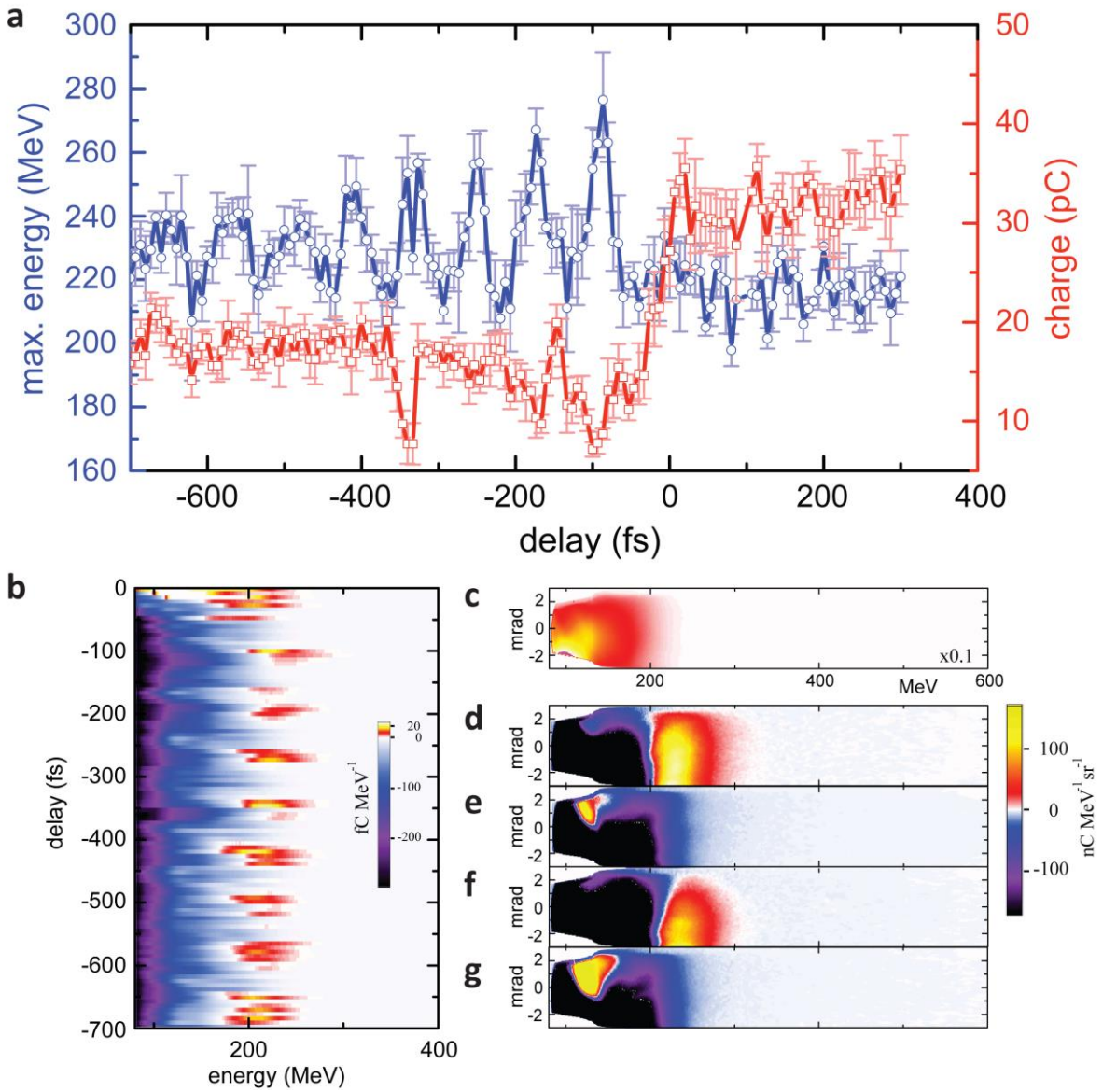

Figure 2 Spectra of electron beams from staged acceleration : (a) maximum electron energy (blue) and total electron beam charge (red) as a function of the delay of the two driving laser pulses. A single data point represents an average of 5 measurements and the error bar the standard deviation. (b) waterfall plot of electron spectra (5-shot average), each with the reference subtracted, as function of delay. (c) 100-shot average unperturbed reference for delays of 100-300 fs before arrival of the second laser pulse. (d)-(g) 2D charge maps (5-shot average) subtracted by the reference (c) for the first two maxima and minima of the energy oscillation shown in (a), i.e. for delays of -107 fs, -153 fs, -193 fs and -240 fs respectively.

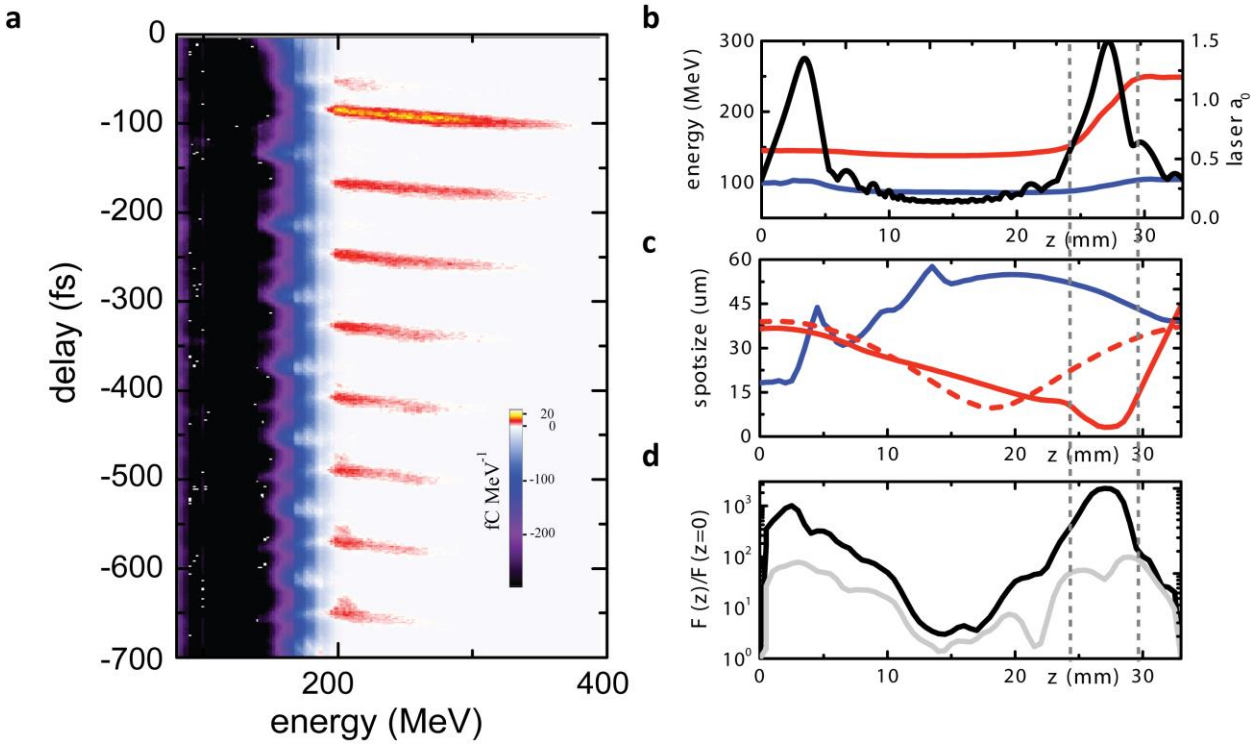

Figure 3 Simulation results: (a) waterfall plot of electron spectra as function of delay with identical colorscale to Fig. 2b. Each spectrum was subtracted by the reference in a similar way as for the experimental results. (b) evolution of the laser intensity expressed as relativistically normalized laser vector potential a_0 (black), evolution of electron energy as function of propagation in the capillary for two different electron populations for a delay of -252 fs: electrons with an initial energy in the interval 75-125 MeV (blue) and electrons with a final energy of 200-300 MeV (red). (c) evolution of the electron beam rms spotsize for the same electron beam subsets as in (b) along with the electron beam rms spotsize of the 'red' electrons without influence of the laser field. (d) total transverse force on the electron beam divided by the contribution from the discharge current for two different distances from the axis: 10 µm (black) and 20 µm (gray) . The area between the grey dashed lines in Fig. b-d indicates where the electrons with final energy >200 MeV are trapped and accelerated in the laser wakefield.

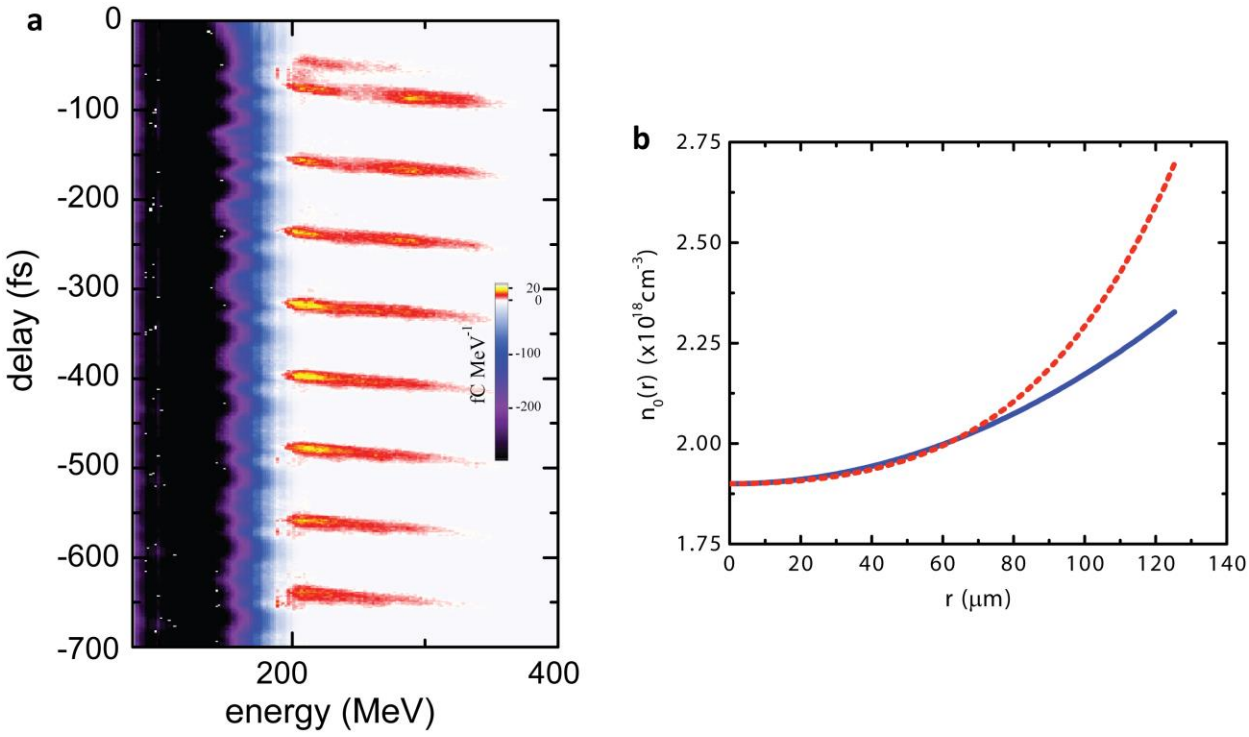

Extended Data Figure 1. Simulation results with quartic transverse plasma density profile. (a) waterfall plot of electron spectra as function of delay with identical colorscale to Fig. 2b. Each spectrum was subtracted by the reference in a similar way as for the experimental result presented in Figs. 1b and 2b. (b) The quartic profile used in the simulation is $n(r) = n_0 + \varepsilon\alpha r^2 + \frac{\alpha}{2}(1-\varepsilon)(\pi\alpha r_e)^{1/2} r^4$, with $\epsilon = 0.7$ (red dashed). The chosen form for the quartic profile is such that for any chosen ϵ $(0 \leq \epsilon \leq 1)$ the matched spotsize in the limit of a low laser power and low laser intensity is the same as for the parabolic profile $\epsilon = 0$ (blue).

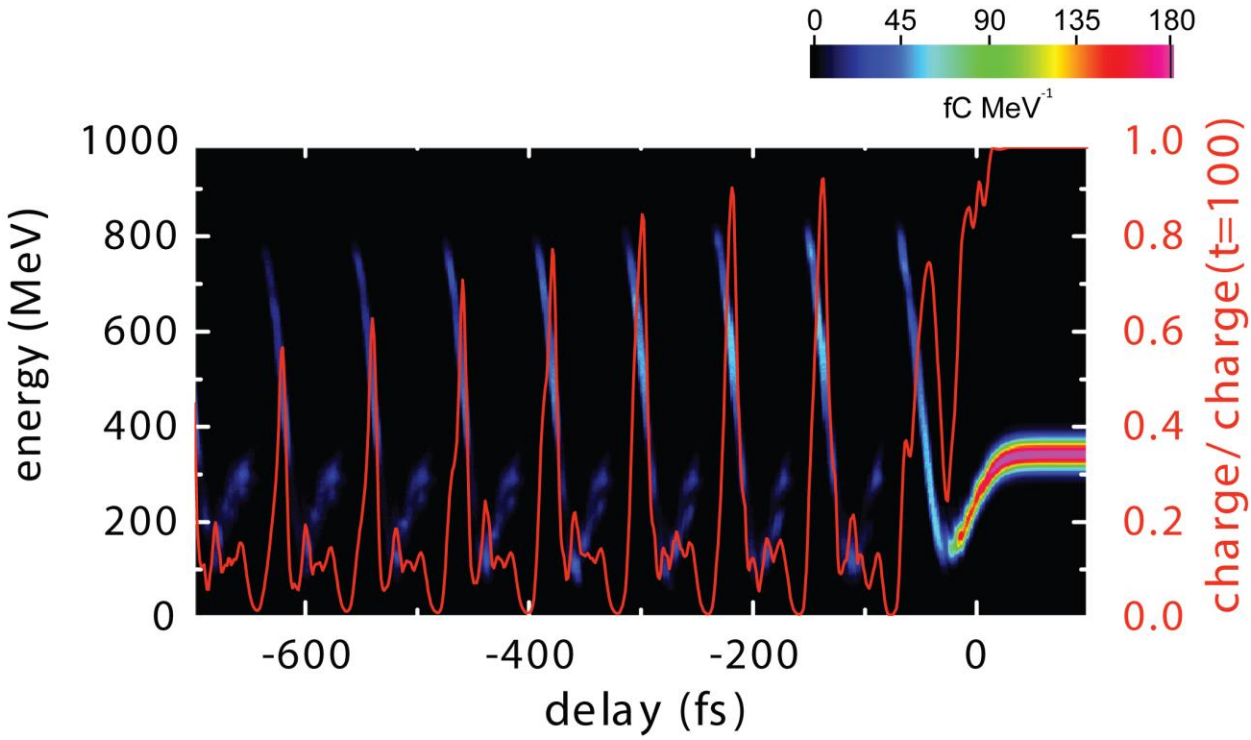

Extended Data Figure 2. Simulation with optimized laser-plasma parameters. The injector electron beam with a central energy of 350 MeV, 10 pC charge, 6 % rms energy spread and a divergence of 2.5 mrad (FWHM) interacting with a 1 J laser pulse and a matched spot size of w_0=40 μm. The red line shows the fraction of trapped charge.

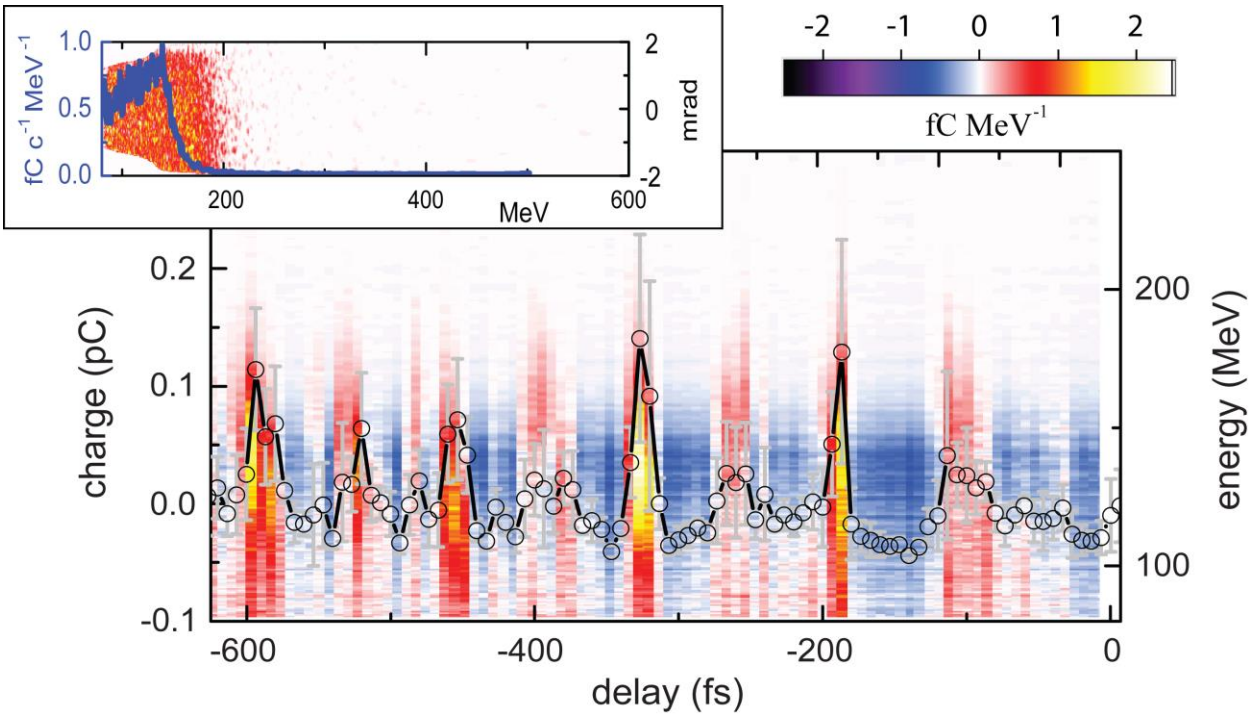

Extended Data Figure 3. Injector beams interacting with the wakefield in the discharge capillary with defocusing current direction of the 2nd LPA stage: waterfall plot of electron spectra subtracted by the reference shown vertically with the charge density in color code and total electron beam charge (black dots). The unperturbed reference beam is shown as inset

Methods

Laser pulses with a center wavelength $\lambda = 0.8\,\mu m$ from the TREX Ti:sapph laser at the BELLA center were split with a MgF_2 beamsplitter of 5mm thickness. For stage 1(2), 70% (30%) of the 40 TW laser pulse energy, i.e. 1.3 J (0.45 J) of laser energy was focused by a 2 m focal length parabola to a beamwaist w_0 = 18 µm. This corresponds to a laser intensity of 4×10^{18} Wcm^{-2} ($1.4 \times 10^{18} Wcm^{-2}$) at a pulse duration of 45 fs.

Plasma Mirror. A feedback-controlled, VHS-tape-based plasma-mirror system (PM) was used to combine the injection beam with the laser driver for the second stage. The electron beam passed through the tape, while the laser beam was reflected at 90 degrees. This PM[24] has a laser energy throughput of 80% (i.e. 480 mJ laser energy), results in no observable laser mode or pointing degradations, and has been fully characterized and improved to provide uninterrupted operation at a repetition rate of 1 Hz for hours of run time.

Electron-beam diagnostic. The energy spectrum of electron bunches emerging from the plasma was measured by a magnetic electron spectrometer. It utilized a 120 mm by 480 mm rectangular-pole electromagnet with the maximum field strength of 1.5 T[30]. Deflected electrons went through scintillating screens (Lanex, Kodak) that were arranged to optimize the energy resolution[31], and the resulting light was imaged by three synchronously triggered CCD cameras, enabling single-shot detection of electrons with energies in the range 0.055–0.25 GeV and 0.3–2.1 GeV for 1T.

Gas jet. A supersonic deLaval nozzle type gas jet with a diameter of 700 µm was used as first stage target. At backing pressures of 150 psi (99%-He, 1%-N2 mixture), the neutral density profile exhibited an approximately Gaussian shape, verified by interferometric measurements[32]. The plasma density at the interaction point with the laser pulse was 5×10^{18} cm^{-3}.

Stage I electron beam. To establish a stable injector stage, 70% of the energy of the BELLA center TREX laser pulse (see Methods) was focused onto a supersonic gas jet (see Methods). A composition of two gases (99% helium and 1% nitrogen) was used to increase the amount of trapped charge. In such a mixed gas, injection was achieved by ionizing deeply bound electron from a high atomic number gas (nitrogen) near the peak of the laser pulse, the proper phase inside the wakefield allowing them to be trapped[33,34]. Stable electron beams with mean energy of (120±5) MeV, 60% (FWHM) energy spread, beam charge of (33±5) pC, and low divergence (4±0.3) mrad were routinely produced with a pointing stability of 0.3 mrad (standard deviation) over hours of run time (corresponding to thousands of laser shots and more than 10 days).

Capillaries. The capillary employed as the active plasma lens had a diameter of 500 µm and length 15 mm. Hydrogen gas was flowed into the capillary through slots located 2 mm from each end of the capillary. The discharge current temporal profile was approximately sinusoidal, with peak current 650 A. Data were taken for laser arrival at the peak of the discharge and allowed focusing of the of 100 MeV electrons to the entrance of the accelerator stage capillary which was located 25mm downstream of the exit of the active plasma lens. The capillary employed as the second stage had diameter of 250 µm and length of 33 mm. Hydrogen gas was flowed into the capillary through slots located 2 mm from each end of the capillary. The discharge current was approximately sinusoidal, with peak current 350 A. Data were taken for laser arrival at the peak of the discharge.
The two discharge capillaries have identical lens strength and form an imaging telescope for the electron beam. It was independently verified that an electron propagating through this imaging telescope, without the influence of the second stage laser pulse, has the same final divergence as the input electron beam, in the range of $60 - 300$ MeV relevant for this experiment.

Numerical modeling. Calculations of the laser–plasma interaction including laser and wakefield evolution, and of electrons acceleration/modulation are carried out with the computational framework INF&RNO[28] (Integrated Fluid and Particle Simulation Code). INF&RNO is a two-dimensional cylindrical (r–z) code that adopts an envelope model for the laser pulse and makes use of the ponderomotive-force approximation to describe the interaction of the laser pulse with the plasma. In

the simulations presented in this work the background plasma is modeled via a (noiseless) cold fluid description, while a fully kinetic description, realized through the particle-in-cell (PIC) approach, is used for the electron bunch. The laser envelope is evolved in time using a second-order Crank–Nicolson method. The full wave operator is retained in the evolution equation for the laser envelope. At any given time step, once the laser envelope is specified, the (fluid) wakefield is computed using a quasi-static approach. The effect of the discharge current in stage II is taken into account by adding a radially varying azimuthal magnetic field corresponding to 325 A discharge current. Time evolution of the electron bunch is computed using a fourth-order Runge-Kutta integrator. The input laser pulse is modeled according to the measured transverse laser intensity profile. The background plasma profile on stage II has a length of 33 mm, with 3 mm initial/final ramps and a 27 mm-long longitudinal flat-top section in the center. The transverse density profile is parabolic with a matched radius r_m=45 μm. The initial (i.e., after the first LPA stage) phase space distribution for the electron bunch is modeled according to the measured bunch properties [see spectrum in Fig. 2c]. The initial bunch length was varied in the range 1-30 μm (longitudinal flat-top profile), while the initial bunch radius was chosen in the range 0.2-5 μm (transverse flat-top profile). Simulation results are insensitive to the choice of the initial bunch radius within the aforementioned range. In each simulation the complete transport of the electron bunch from the exit of stage I to the entrance of stage II is modeled, including the effect of the active plasma lens (powered with a current of 650 A) and the interaction (scattering) with the plasma-mirror tape. The final (i.e., after stage II) electron spectra have been computed taking into account the finite acceptance of the spectrometer.

Additional references

30 Nakamura, K. *et al.* Broadband single-shot electron spectrometer for GeV-class laser-plasma-based accelerators. *Review of Scientific Instruments* **79**, 053301, (2008).

31 Nakamura, K. *et al.* Electron beam charge diagnostics for laser plasma accelerators. *Physical Review Special Topics - Accelerators and Beams* **14**, 062801, (2011).

32 Plateau, G. R. *et al.* Wavefront-sensor-based electron density measurements for laser-plasma accelerators. *Review of Scientific Instruments* **81**, 033108, (2010).

33 Rowlands-Rees, T. P. *et al.* Laser-driven acceleration of electrons in a partially ionized plasma channel. *Physical Review Letters* **100**, 105005, (2008).

34 Chen, M., Esarey, E., Schroeder, C. B., Geddes, C. G. R. & Leemans, W. P. Theory of ionization-induced trapping in laser-plasma accelerators. *Physics of Plasmas* **19**, 033101, (2012).